

G-quadruplex identification in the genome of protozoan parasites points to naphthalene diimide ligands as new antiparasitic agents

Efres Belmonte-Reche,[†] Marta Martínez-García,[†] Aurore Guédin,[‡] Michela Zuffo,^{||} Matilde Arévalo-Ruiz,[†] Filippo Doria,^{||} Jenny Campos-Salinas,[†] Marjorie Maynadier,[⊥] José Juan López-Rubio,[#] Mauro Freccero,^{||} Jean-Louis Mergny,^{‡,†} José María Pérez-Victoria,^{†,*} and Juan Carlos Morales^{†,*}

Affiliations:

[†] Department of Biochemistry and Molecular Pharmacology, Instituto de Parasitología y Biomedicina, CSIC, PTS Granada, Avda. del Conocimiento, 17, 18016 Armilla, Granada, Spain.

[‡] ARNA laboratory, Université de Bordeaux, Inserm U1212, CNRS UMR5320, Institut Européen de Chimie Biologie (IECB), 2 rue Robert Escarpit, 33607 Pessac, France.

^{||} Department of Chemistry, University of Pavia, V.le Taramelli 10, 27100 Pavia, Italy.

[⊥] Dynamique des Interactions Membranaires Normales et Pathologiques, CNRS UMR 5235, Université de Montpellier, 34095 Montpellier, France.

[#] CNRS - 5290, IRD 224 - University of Montpellier (UMR 'MiVEGEC'), INSERM, 34394 Montpellier, France.

[†] Institute of Biophysics, AS CR, v.v.i. Kralovopolska 135, 612 65 Brno, Czech Republic.

ABSTRACT

G-quadruplexes (G4) are DNA secondary structures which take part in the regulation of gene expression. Putative G4 forming sequences (PQS) have been reported in mammals, yeast, bacteria and viruses. Here, we present PQS searches on the genomes of *T. brucei*, *L. major* and *P. falciparum*. We found telomeric sequences and new PQS motifs. Biophysical experiments showed that EBR1, a 29 nucleotide long highly repeated PQS in *T. brucei*, forms a stable G4 structure. G4 ligands based on carbohydrate conjugated naphthalene diimides (carb-NDIs) which bind G4's including hTel, could bind EBR1 with selectivity versus dsDNA. These ligands showed important antiparasitic activity. IC₅₀ values were in the nanomolar range against *T. brucei* with high selectivity against MRC-5 human cells. Confocal microscopy confirmed these ligands localize in the nucleus and kinetoplast of *T. brucei* suggesting they can reach their potential G4 targets. Cytotoxicity and zebrafish toxicity studies revealed sugar conjugation reduces NDIs intrinsic toxicity.

INTRODUCTION

G-quadruplexes (G4) are secondary structures formed by guanine-rich DNA and RNA sequences. Their basic motif is a four guanine tetrad linked through Hoogsteen hydrogen bonding that stacks on top of other G-tetrads helped by interactions with cations, such as Na⁺ or K⁺. G4 topologies are quite diverse and depend on base sequence, loop connectivity and the *syn* or *anti* guanine configuration along the oligonucleotide folding.¹

G4 sequences are overrepresented in certain key regions of the genome² such as promoters, enhancers, insulators, origins of replications and telomeres. These findings suggest that G4 have important functions in cellular and genetic processes. Visualization and genome mapping experiments³ suggest that G-quadruplex DNA can be formed when DNA single strands are exposed during replication or transcription. G4 structures pose challenges to replication and G4 helicases are essential to unwind them and thus maintain genetic stability.⁴ Sarkies *et al.* also suggested that G4 DNA are involved in the maintenance of epigenetic regulation of gene expression.⁵

Putative G-quadruplex sequences (PQS) have been found in organisms other than humans, such as other mammals,⁶ yeast,⁷ bacteria⁸ and viruses.⁹ In contrast, few data have been reported of G4 in parasites.¹⁰ The malaria-causing parasite *Plasmodium falciparum* has an extremely AT rich DNA (> 80 %) which, in principle, lowers the possibilities of G4 formation.¹¹ Nevertheless, successive bioinformatic searches have identified several putative quadruplex sequences (PQS),^{10, 12} which may play a role in antigenic variation and diversification.^{10, 12a} Bottius *et al.*¹³ reported the existence of a common degenerate motif GGGTTYA (where Y is T or C, PfTel) in the DNA of *P. falciparum* and localized it mainly in the 1.3 kb (average) telomeric regions of the parasite chromosomes. This degenerate motif has also been found in other *Plasmodium* species.¹⁴ Interestingly, its repetitive sequence being different from the human telomeric one (GGGTTA; hTel), in principle gives the opportunity of a selective targeting. These repeats and other G4 forming sequences are abundant in *var* gene regulatory regions.^{10, 12, 15} The *var* genes, which regularly recombine to generate new variants,¹⁶ code for PfEMP1, a family of variant surface antigens responsible for preventing the infected erythrocytes from being recognized by the host's immune system by continuously presenting different PfEMP1 proteins.¹⁷ This phenomenon of antigenic variation is produced because the parasite expresses an exclusive PfEMP1 protein but frequently switches to express different *var* genes.¹⁷ The

presence of G4 sequences in *var* gene regulatory regions has been suggested to influence *var* gene recombination and/or switching.^{12a}

Potential G4 sequences have been scarcely investigated in parasites of the *Trypanosomatidae* order. *Trypanosoma brucei* and *Leishmania major* are responsible for two life-threatening neglected diseases, sleeping sickness (or African Trypanosomiasis) and Leishmaniasis, respectively. Both species present telomeric regions with tandem repetitions of the hTel sequence¹⁸ and their variability has been related with gene expression critical for their survival, chromosomic polymorphisms and rearrangements.¹⁹ In these telomeric regions G-rich sequences facilitate the switching of the important variable surface glycoprotein (VSG) genes,^{10, 20} which are responsible for the antigenic variation that this parasite uses to evade the immune system.²¹ However, the direct involvement of quadruplexes in this process has yet to be established. On the other hand, *T. brucei* presents a single mitochondrion of which the genome, also known as kinetoplastid DNA, contains several open reading frames (ORF) that require editing to become translatable mRNAs.²² Nine of these ORF's are pan-edited, leading to the site-specific insertion and deletion of hundreds of U-nucleotides.²³ Recently, 27 PQS were detected in eight of the nine pan-edited mitochondrial pre-mRNA transcripts of *T. brucei*.²³ Interestingly, the stepwise editing of these pre-mRNAs progressively resolves these G4 structures generating less structured ORF's, suggesting that they could be due to an evolutionary driving force for RNA editing in trypanosomes.²³

Drugs currently used to treat neglected diseases have limited efficacy, are hampered by appearance of resistance and/or are toxic. There is therefore an urgent need to find new targets for the development of drugs,²⁴ and G4 could be an attractive alternative target. In fact, due to their roles in a number of biological processes, G4 have been proposed as potential therapeutic targets in cancer²⁵ and small molecule G4 ligands have been reported for the last two decades as antitumor drugs.^{4d, 26} G4 have also been suggested as targets for treating virus such as HIV and several G4 ligands have been reported as potential drugs.²⁷ In the case of parasites, De Cian *et al.*²⁸ reported that several classical G4 ligands such as BRACO-19, TMPyP4, PIPER, telomestatin and others were capable of binding the degenerative motif of *P. falciparum* telomere GGGTTYA. Actually, the Phen-DC family exhibited the most noticeable stabilization effect over all three PFTel tested, yet failed -as all the other compounds used- to discriminate against the hTel sequence. Similarly, the bis-quinacridine BOQ1 ligand showed binding to the UpsB-Q G-quadruplex, a G4 formed in an upstream regions of groupB *var* genes of *P. falciparum*.^{12b} Recently, a bis-pyrrolo[1,2-a]quinoxaline

family of compounds has been described to bind two PflTel G4 sequences and to display antimalarial activity,²⁹ and TMPyP4 and Telomestatin were reported to inhibit 50% growth of *P. falciparum* at 5 and 35 μM concentration, respectively.³⁰ To the best of our knowledge, these are the only reported examples of G4 ligands with antiparasitic activity.

In a previous work we synthesized and evaluated a new family of carbohydrate naphthalene diimide derivatives (carb-NDI) as G4-binders and antitumor drugs (Figure 1).³¹ The binding results to G4 targets and nuclear localization in cells suggested that this family of ligands interacts with G4 structures.

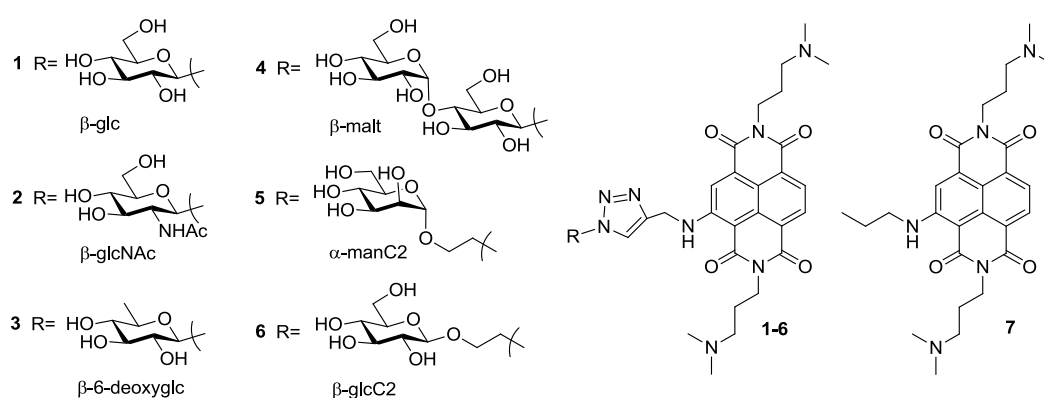


Figure 1. Carb-NDI family of G-quadruplex ligands studied in this work.

The initial purpose of using sugar-conjugated anticancer drugs was to take advantage of the Warburg effect and the over-expression of GLUT transporters in cancer cells due to the high energy requirements.³² We envisioned that sugar-conjugation in antiparasitic drugs could be useful for a better uptake of the drug in the parasite. In fact, glucose transporters play a central role in their survival. The LGT family of transporters of *Leishmania spp.*³³ relates to the human GLUT1 in sequence and structure and have higher glucose affinity than the human counterpart.³⁴ Additionally, they have been found to be critical for parasite survival since LGT null mutants are more susceptible to oxidative stress and have reduced viability at high temperatures or under nutrient deficiency.³⁵ In *Plasmodium falciparum*, the PfHT1 protein has significant sequence identity to the human GLUT1³⁶ and broad specificity for hexoses. The main sugar transporter identified in the bloodstream form of *Trypanosoma brucei* is THT1 which is a low-affinity and high-capacity facilitative protein that takes advantage of the high concentration of glucose in the blood.³⁷

In this work, we have made a genomic search of PQS for *T. brucei*, *L. major* and *P. falciparum*. We have localized G4 sequences in their genomes and evaluated their possible importance for the parasite survival. We have evaluated a unique G4 sequence found in *T. brucei* (EBR1) for its ability to form stable G-quadruplex using biophysical methods. Furthermore, the carbohydrate-NDIs have been investigated as potential ligands of EBR1 and evaluated as antitrypanosomal, antileishmanial and antimalarial agents together with their toxicity in human cells and in zebrafish embryo. Finally, location of carb-NDIs inside *T. brucei* and *Leishmania*, and their potential effect on parasitic gene expression were also studied.

RESULTS AND DISCUSSION

Putative G-quadruplex sequences (PQS) search in *T. brucei*, *P. falciparum* and *L. major* genomes. The possibility of G-quadruplex formation was analyzed using the online algorithm software for PQS-search engine called QGRS Mapper since it is user-friendly, commonly used algorithm.³⁸ The genomes were downloaded from tritrypDB (<http://tritrypdb.org> for *T. brucei* V. 5.1 accessed Jan-2016), the Sanger Institute (<http://www.sanger.ac.uk> for *L. major* V. 6.1 accessed June-2016) and from plasmoDB (<http://plasmodb.org> for *P. falciparum* V. 3.0 accessed Jan-2016) and only the positive strands were included. The results were set to leave out overlapping PQS. Additional parameters were set to default, (max length= 30, min G-group size=3, loop size=3-10). With these parameters, 466 PQS were found for *P. falciparum*, whereas Smargiasso *et al.*^{12b} reported 891 PQS when searching through the whole genome. The resulting variation is probably due to the differences in the parameter criteria (Smargiasso used a loop range of 0 to 11) and in the genome version. A similar number of PQS (433) was also detected in *T. brucei*, although its genome is larger than the one of *P. falciparum* (32 vs 23 Mbp) and its composition is more GC-rich (45% *T. brucei*, 20% *P. falciparum*). *L. major* displayed 4719 PQS, ten times more than *T. brucei*, despite having similar genomic size and a composition of 57% GC. Both of these genomic parameters cannot explain the big difference in PQS detection rates. These tendencies were better observed when comparing parasite PQS densities (number of PQS/10.000 bases) 0.15, 0.24 and 1.42 for *T. brucei*, *P. falciparum* and *L. major*, respectively. Large differences were also observed between chromosomes. *L. major*'s chromosomes 4, 13, 17, 34 and 36 displayed very high PQS concentration while chromosomes 12 and 14 of *P. falciparum* have a very low density of G4-prone sequences (Table S2). *T. brucei* displayed low PQS concentration in its entire genome.

The relevance of the PQS found can be estimated based on the G-score, a validation system on QGRS-mapper. The algorithm tends to emphasize shorter loops with equal size and higher number of guanine tetrads. However, false positives (where high G-score PQS are unable to form G4) and false negatives (where low G-score PQS are able to form stable G4) are given sometimes as results. To solve these potential errors, several other algorithms have been developed, such as G4-hunter.^{1e} G4-hunter validates PQS ability to form G4 by taking into account G-richness (G in sequence) and skewness (G/C asymmetry with the complementary strand) of the PQS area and thus drastically reduces false results. We decided to validate PQS results simply by frequency. Higher frequencies are in principle less prone to be random nucleotide sequences without a biological role. At the same time, all highly-frequent PQS found for the examined parasites are verified G4-forming sequences. For *L. major* and *T. brucei* these PQS include the hTel sequence, and for *P. falciparum* the variety of PfTel sequences (Table 1). In *T. brucei* we also found a highly frequent new non-telomeric sequence which however was given a poor G-Score by the search engine. This sequence (EBR1) was found 33 times (Table 1).

Table 1. Most frequent PQS found in *L. major*, *T. brucei* and *P. falciparum* genomes and number of occurrences. Frequency is the number of times the sequence occurs in the genome.

	PQS	Name	Frequency
<i>L. major</i>	GGGTTAGGGTTAGGGTTAGGG	hTel	465
	GGGAGGGAGGGAGGG		26
	GGGTGAGCGGGTGGGGTCAGTGGG		22
	GGGGTGGGCCACGCGGGACAGGACGGG		21
	GGGCGTGGGTGTGGGTGTGGG		19
	GGGCGAGGGGGAGGGGGTGCTGGG		17
	GGGAAAAGAAGGGGAAGGGGTAGGG		16
	GGGTGGGTGGGTGGG	T30693	16
<i>T. brucei</i>	GGGCAGGGGGTGATGGGGAGGAGCCAGGG	EBR1	33
	GGGTTAGGGTTAGGGTTAGGG	hTel	26
	GGGAGAGGGAGAGGGAGAGGG		5
<i>P. falciparum</i>	GGGTTTAGGGTTCAGGGTTTAGGG	PfTel	84
	GGGTTTAGGGTTTAGGGTTTAGGG	PfTel	67
	GGGTTCAGGGTTTAGGGTTCAGGG	PfTel	63
	GGGTTTAGGGTTTAGGGTTCAGGG	PfTel	63
	GGGTTCAGGGTTTAGGGTTTAGGG	PfTel	58
	GGGTTTAGGGTTCAGGGTTCAGGG	PfTel	26
	GGGTTCAGGGTTCAGGGTTTAGGG	PfTel	19

When we checked the location of EBR1 in *T. brucei* genome we found it was repeated 22 times in between percentile 34.2 and 35.2 of chromosome 9, where it located inside several genes coding, among others, for a purine nucleoside transporter (NT10), a calpain-like cysteine peptidase, an adenylosuccinate lyase and other proteins with unknown function. The rest of EBR1 sequences were found in between percentile 6.6 and 6.9 of chromosome 11 and inside a gene coding for an iron/ascorbate oxidoreductase. The hTel sequences in *L. major* and *T. brucei* were mainly localized in the telomeric regions as expected. For *T. brucei*, some of these sequences were found to be in or in between VSG genes, yet also throughout non-telomeric areas affecting a trans-sialidase neuraminidase and several unknown proteins. PfTel sequences found in *P. falciparum* were mostly localized in the telomeric areas (percentile > 99.9) and affecting PfEMP1 expressing genes as it was reported earlier.

G4 formation by *T. brucei* EBR1 sequence. Due to the novelty and frequency number in *T. brucei* genome, the EBR1 sequence (Table 1) was selected and analyzed for its ability to form G-quadruplex. Circular dichroism (CD) spectroscopy was first carried out in the absence and presence of increasing concentrations of K⁺ to investigate G-quadruplex formation.³⁹ EBR1 CD spectra showed positive signals at 260 and 295 nm, and a negative signal at 240 nm suggesting a predominantly parallel G-quadruplex conformation (Figure 2a). When CD was recorded in sodium buffer conditions the spectra were similar but with lower intensity (Figure S1). It is important to mention that G4 seems to be partially folded even in the absence of cations (Figure S1) and CD signals increase with accumulative amount of cations. Other examples have been reported of G4 formation in the absence or low concentration of monovalent cations.⁴⁰ A mutated EBR1 sequence (EBR1-mut) where several guanine residues were changed to adenine or thymine was also examined for comparison (Figure S2). In this case, no CD signals characteristic of G-quadruplex formation were detected and only small changes were observed after K⁺ or Na⁺ addition.

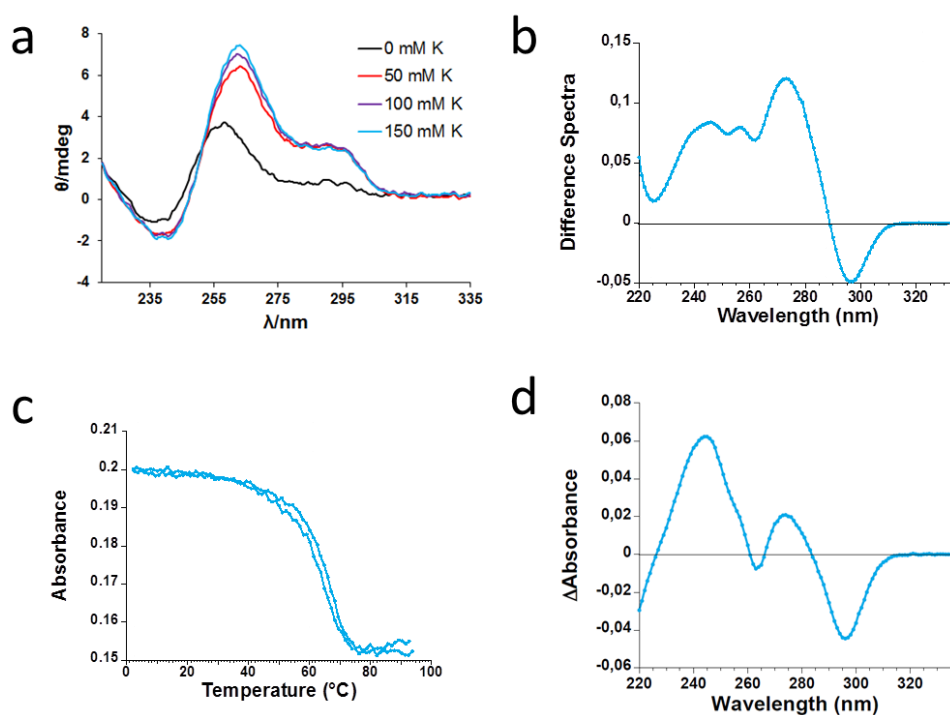


Figure 2. Characterization of EBR1 sequence. a) CD spectra in the absence and presence of different concentrations of K^+ . b) Thermal difference spectra (TDS). c) UV-monitored thermal denaturation experiment at 295 nm. d) Isothermal difference spectra at 25°C (IDS).

UV thermal difference spectroscopy (TDS)⁴¹ were recorded on EBR1 (Figure 2b) by subtracting spectra at 93.5 and at 2.7 °C. Major positive peaks at 247, 257 and 274 nm, together with a negative peak at 296 nm are a typical signature of G-quadruplex folding. UV melting⁴² of EBR1 monitored at 295 nm showed the usual negative sigmoidal curve for G-quadruplex with a T_m value of 65 °C (Figure 2c). The reverse cooling experiment showed an almost overlapping curve (Figure 2c). IDS spectra on EBR1 were obtained by taking the difference between the absorbance spectra of folded and unfolded oligonucleotides. These spectra were respectively recorded before and after potassium cation addition (100 mM KCl) at 25°C. (Figure 2d) This signature is characteristic of a G4 structure, as in the case of the TDS spectra. The spectra showed major positive peaks at 244 and 274 nm with a negative peak at 296 nm.

Proton NMR experiments were run on the unlabeled EBR1 sequence at 25 and 60°C, close to the T_m measured by UV melting. Both spectra displayed the characteristic imino peaks in the 10-12 ppm range and none at higher field (Figure S3), suggesting the exclusive folding into G4 structures.⁴³ However, the spectra displayed a complex mixture of signals, indicating the coexistence of more than one conformation. Even

close to the melting temperature a favoured one could not be identified, suggesting that they all have similar stability.

After validation of EBR1 folding into a G4 structure, we proceeded to test ligand binding. FAM and TAMRA fluorophores were attached to the 5'- and 3'-ends of EBR1 sequence (EBR1-FT, see Table S1) to run FRET experiments. Preliminary UV melting and CD experiments were carried out on EBR1-FT. The results demonstrated that the stability and folding topology are in good agreement with those obtained for the unlabeled EBR1 sequence (Figure S4).

Next, two of our G-quadruplex ligands, the carb-NDI **6** and the reference aglycone-NDI (**7**) were tested for binding to the EBR1 G4 structure using FRET. Carb-NDIs **1-6** and aglycone NDI **7** have previously shown binding to several G-quadruplex structures (hTel, c-myc, human minisatellite and Bombyx telomere) with certain selectivity for quadruplexes over DNA duplexes.³¹ FRET-based melting assays were performed in the presence of 10 and 50 mM concentrations of K⁺, with 0.5, 1 and 2 μM of compounds **6** or **7** and 0.2 μM of the oligonucleotide. Both compounds showed binding to EBR1 and ΔT_m values were higher for aglycone-NDI **7** than for glcC2-NDI **6** (Figure 3a and Figures S5). This tendency had been observed previously for the same ligands **6** and **7** when binding to other G4 structures. Yet, ΔT_m values obtained for EBR1 were lower than those seen with the hTel sequence (at 10 mM of K⁺ and 2 μM of compound, 19 °C for compound **7** and 10 °C for compound **6**). CD titrations with carb-NDIs **6** and **7** on EBR1 also confirmed binding (Figure 3b and 3c). An increase on the 290 nm band and a decrease in the 265 nm band were clearly observed upon addition of increasing concentrations of the ligands. These binding results indicate that ligands **6** and **7** not only bind to the *T.brucei* telomeric sequence but also to other G4 structures found within the *T.brucei* genome.

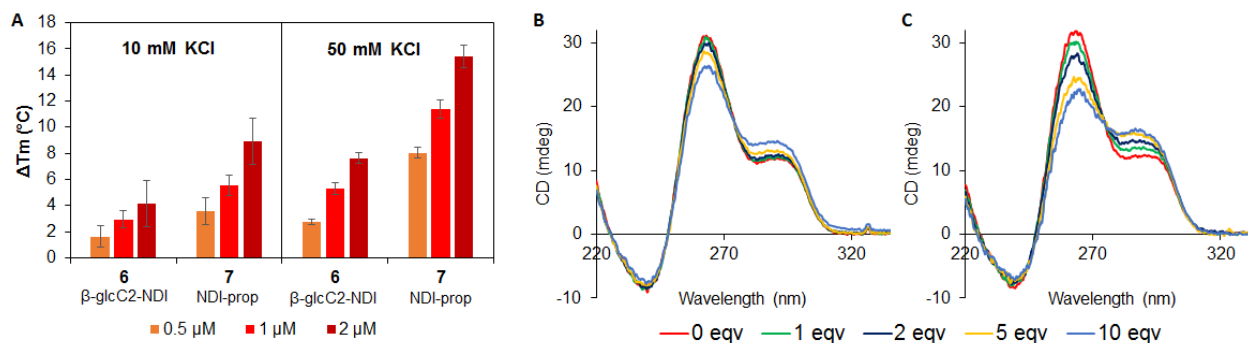


Figure 3. a) FRET-melting assay. Thermal stabilization induced by the tested compounds **6** and **7** (0.5, 1 and 2 μM) on the EBR1-FT (fluorescently-labeled) quadruplex (0.2 μM) in 10 mM lithium cacodylate pH 7.2 containing 10 mM KCl + 90 mM LiCl or 50 mM KCl + 50 mM LiCl. b) CD titration of compound **6** on the EBR1-FT quadruplex (3 μM) in 10 mM lithium cacodylate (pH 7.2) containing 100 mM KCl. c) CD titration of compound **7** on the EBR1-FT quadruplex (3 μM) in 10 mM lithium cacodylate (pH 7.2) containing 100 mM KCl.

Antiparasitic activity and toxicity of G4 ligands. The *in vitro* antiparasitic activities of carb-NDI G4 ligands (**1-7**) were evaluated against bloodstream forms of *T. brucei brucei*, against promastigotes of *L. major* and against *P. falciparum* (Table 2). Cytotoxicity values of these compounds against a human non-tumoral lung cell line (MRC-5) were recently reported and are also included in the table.³¹ Selectivity indices (SI) were calculated according to the formula: $IC_{50}(\text{MRC-5}) / IC_{50}(\text{parasite})$. Pyridostatin, BRACO-19 and TmPyP4 were used as alternative G-quadruplex ligands for comparison in *T. brucei* and *P. falciparum*. Suramin, miltefosine and chloroquine were used as positive drug controls for *T. brucei*, *L. major* and *P. falciparum*, respectively.

Carb-NDI G4 ligands (**1-6**) presented the best antiparasitic activity against *T. brucei* with IC_{50} values between 17 and 24 nM, except for compounds **2** and **4** which were slightly less potent (89 and 99 nM, respectively). Compounds **1-6** were more effective against *T. brucei* than against HT-29, MCF-7 and HeLa cancer cells (IC_{50} values from 0.1 to 2.9 μM), with aglycone-NDI **7** displaying the lowest IC_{50} of the series in a similar way to the tendency found in cancerous cells.³¹ IC_{50} values for most of these G-quadruplex ligands are in the same range as that of the commercial drug suramin, used to treat sleeping sickness. At the same time, the selectivity indexes ($IC_{50}(\text{MRC-5}) / IC_{50}(\text{parasite})$) for compounds **1-7** were quite high ranging from

38.6 to 53.5, except for compounds **2** and **4** (5.7 and 20.6, respectively). It is important to note that classical G-quadruplex ligands such as pyridostatin, BRACO-19 and TMPyP4 showed IC₅₀ values in the micromolar range, far higher than those obtained for compounds **1-7**. Differences in drug uptake and/or binding to specific G4 targets such as EBR1 may explain these data.

Table 2. Compound antiparasitic activity against all three parasites and cytotoxicity values for MRC5 control cell line of the G4 ligands **1-7** plus three classical G4 binders. Selectivity values are also shown.

	IC ₅₀ Parasites (μM)				SI		
	<i>L. major</i>	<i>T. brucei</i>	<i>P. falciparum</i>	MRC-5†	<i>L. major</i>	<i>T. brucei</i>	<i>P. falciparum</i>
1 β-glc-NDI	0.244 ± 0.007	0.024 ± 0.001	1.350 ± 0.636	1.15 ± 0.29	4.7	47.9	0.9
2 β-glcNAc-NDI	1.041 ± 0.027	0.089 ± 0.007	0.360 ± 0.071	0.51 ± 0.01	0.5	5.7	1.4
3 β-6dglc-NDI	0.184 ± 0.009	0.017 ± 0.007	0.225 ± 0.120	0.91 ± 0.32	4.9	53.5	4.0
4 β-malt-NDI	0.921 ± 0.051	0.099 ± 0.010	0.370 ± 0.085	2.04 ± 0.05	2.2	20.6	5.5
5 α-manC2-NDI	0.306 ± 0.019	0.021 ± 0.003	0.180 ± 0.099	0.81 ± 0.44	2.6	38.6	4.5
6 β-glcC2-NDI	0.537 ± 0.030	0.017 ± 0.009	0.275 ± 0.191	0.71 ± 0.25	1.3	41.8	2.6
7 NDI-prop	0.034 ± 0.005	0.009 ± 0.001	0.091 ± 0.013	0.36 ± 0.16	10.6	40.0	4.0
Pyridostatin	5.00 ± 0.01	7.82 ± 0.20	2.65 ± 1.77	5.38 ± 0.07	1.1	0.7	2.0
BRACO-19	12.73 ± 0.47	5.51 ± 0.99	9.70 ± 4.67	8.33 ± 2.96	0.7	1.5	0.9
TMPyP4	20.82 ± 4.86	>10	>25	>25	>1.7		
Chloroquine			0.0096 ± 0.003				
Suramin		0.038 ± 0.003					
Miltefosine	6.07 ± 0.37						

SI = Selectivity Index (IC₅₀ MRC-5 / IC₅₀ parasite). † From reference 30.

In the case of *L. major* and *P. falciparum*, all IC₅₀ values for Carb-NDI G4 ligands (**1-6**) and aglycone NDI (**7**) were higher than those found for *T. brucei*, although most of them remain in the submicromolar range. This lower effect could be due to differences in drug uptake by the different parasites. Again, aglycone-NDI **7** showed the best antiparasitic activity of the series in both cases, with the carb-NDI presenting slightly higher values (5-30 fold in *L. major* and 2-15 fold in *P. falciparum*). The selectivity index of ligands **1-7** was smaller for these two parasites ranging from 0.5 to 10.6 for *L. major* and from 0.9 to 5.5 for *P. falciparum*. We had previously observed differences in antitumor activity depending on how the carbohydrate was attached to the NDI core.³¹ For example, compound **6** where the glucose is attached through an ethyl spacer is approx. 10 fold more active than compound **1** where is directly attached to the core. In the case of their antiparasitic activity, the sugar presentation in the carb-NDI did not show differences except for *P. falciparum* where compound **6** was fivefold more active than compound **1**. Lastly,

the classical G-quadruplex ligands investigated in *L. major* and *P. falciparum* (pyridostatin, BRACO-19 and TMPyP4) displayed IC₅₀ values in the micromolar range, being quite less potent than ligands **1-7**.

Next, taken advantage of the intrinsic fluorescence of NDI derivatives β -glcC2-NDI **6** (λ_{em} 578 nm, exciting at the maximum absorbance, λ_{exc} 517 nm, in buffered conditions at pH 7.4, Figure S6) and aglycone-NDI **7** (λ_{em} 598 nm, λ_{exc} 538 nm, Figure S6), we investigated their localization in *T. brucei* by confocal microscopy. After 30 min of incubation at 37 °C, both compounds were detected inside the parasites and aglycone-NDI **7** was mainly found in the nucleus and in the kinetoplast (Figure 4). When longer incubation times (150 min) were used both compounds localized mainly in the nucleus and in the kinetoplast. We had previously observed a similar uptake trend in HT-29 colon cancer cells and MRC-5 non-cancerous cells³¹ where aglycone-NDI **7** entered more rapidly into the cells than carb-NDI derivatives, but at longer times all compounds eventually localized within the nucleus. These results suggest that such G4-ligands could reach and possibly target G-quadruplex structures found in the parasite's genome, such as the telomeric sequence and/or EBR1 sequence.

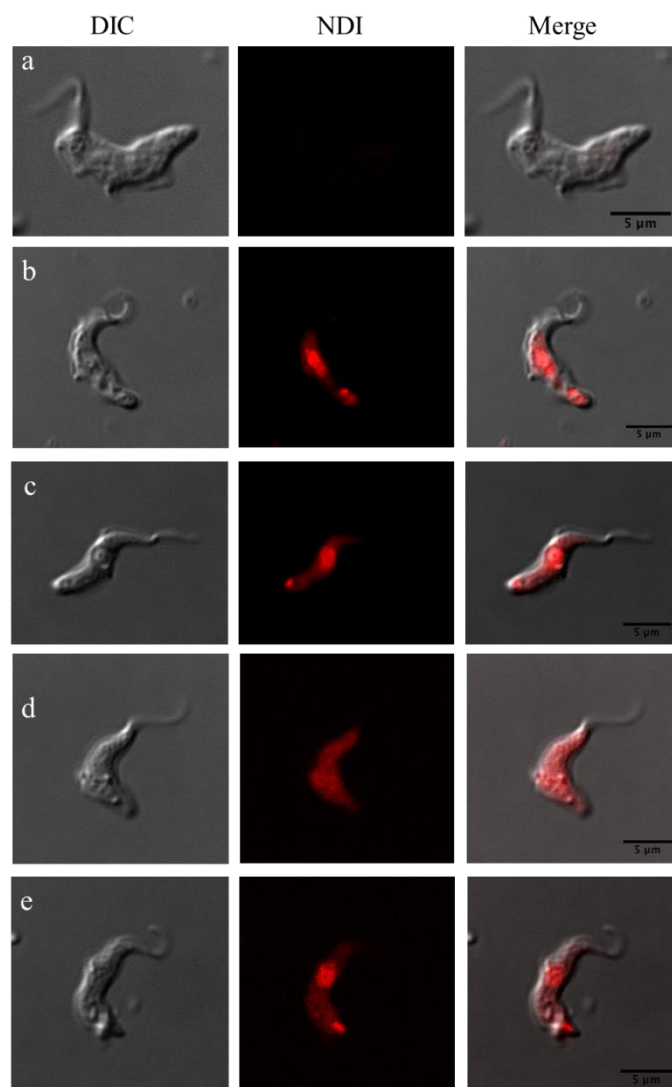


Figure 4. Confocal images of *T. brucei* parasites after incubation at 5 μ M concentration with aglycone-NDI **7** for 30 min (b) or 150 min (c) and with β -glcC2-NDI **6** for 30 min (d) or 150 min (e). Control parasites are shown in (a). Scale bar: 5 μ m.

As G-quadruplex ligands **1-7** have shown nanomolar activity against *T. brucei* and selectivity indexes higher than 40, we decided to perform preliminary toxicity assays in the zebrafish embryo model before future investigation in a mice model of the disease. High fecundity, rapid embryonic development, and high homology to mammalian species make zebrafish a cost-effective model for toxicity screening.⁴⁴ Moreover, the embryo is preferred to adult fish because it is predicted that early life stages feel less pain and distress than adult fish. Fast acute toxicity was measured by incubation of zebrafish embryos with increasing concentration of each compound and cumulative mortality/toxicity was observed after 96 hpf (hours post

fertilization).⁴⁵ It is important to note that cumulative mortality/toxicity is due to both developmental impact and organotoxicity. This methodology is becoming more frequently used by medicinal chemists.⁴⁶

Table 3 shows NOEC, LOEC and LC₅₀ values for acute toxicity on zebrafish embryos and calculated LD₅₀ values on mice for G-quadruplex ligands **1-7**. Conversion of LC₅₀ values on zebrafish embryo to LD₅₀ values on mice was carried out by correlation as suggested by Ali *et al.*⁴⁷ after a large-scale comparison of toxicity in both animal models for 60 water-soluble compounds (Table 3). Interestingly, β-6dglc-NDI (**3**) and β-malt-NDI (**4**), two compounds with low toxicity on MRC-5 cells, were estimated to be the most toxic compounds in mice. On the contrary, glucose or mannose conjugation to the aglycone NDI-prop (such as in compounds **5** and **6**) seems to mitigate the unspecific toxicity associated to these naphthalene diimide ligands. These results point to the relevance that carbohydrate conjugation of G-quadruplex ligands may have on the final toxicity of the compound.

Table 3: NOEC, LOEC and LC₅₀ values for acute toxicity on zebrafish embryos and calculated LD₅₀ values on mice for G-quadruplex ligands 1-7.

Compound	NOEC (μM)	LOEC (μM)	LC ₅₀ (mmol/L)	LD ₅₀ † (mmol/kg) mice	LD ₅₀ † (mg/kg) mice
(1) β-glc-NDI	100	N.A.	> 1	> 0.63	> 580
(2) β-glcNAc-NDI	100	N.A.	> 1	> 0.63	> 607
(3) β-6dglc-NDI	100	N.A.	0.17	0.17	154
(4) β-malt-NDI	100	N.A.	0.19	0.19	206
(5) β-manC2-NDI	100	N.A.	> 1	> 0.63	> 609
(6) β-glcC2-NDI	100	N.A.	> 1	> 0.63	> 609
(7) NDI-prop	100	1000	0.41	0.33	178

LC₅₀ (median lethal dose), calculated by fitting sigmoidal curve to mortality data ($y = \text{Bot} + (\text{Top} - \text{Bot}) / (1 + 10^{-k(x - \text{LC}_{50})})$). Bot, minimum mortality; Top, maximum mortality; k, curve slope; x0, LC₅₀ estimated. NOEC (No observed effect concentration, with mortality score > 20% assumed as the effect). LOEC (Lowest observed effect concentration, with mortality score > 20% assumed as the effect). † Extrapolated according to reference 43.

CONCLUSIONS

Increasing evidence suggests that G4 plays an important role in gene regulation in many organisms. Here, we completed PQS searches on the genome of *T. brucei*, *L. major* and *P. falciparum*. Several interesting PQS were found, including EBR1 on *T. brucei*, which was also confirmed to form stable G4 structures through biophysical assays. The hTel sequences were also found abundantly in the trypanosomatid parasites in long islands of repetitions.

G-quadruplex ligands such as β -glcC2-NDI **6** and aglycone-NDI **7**, which were previously reported to bind to several G4 structures including hTel, were also capable of binding EBR1 G4, found only in the *T. brucei*. At the same time, the carb-NDI family and the aglycone NDI prop **7** showed antiparasitic activity against *T. brucei*, *L. major* and *P. falciparum*. These G-quadruplex ligands were especially effective against *T. brucei* where they also showed a quite high selectivity versus the human control cell line MRC-5. Confocal microscopy studies localized β -glcC2-NDI **6** and aglycone-NDI **7** in the nucleus and kinetoplast of *T. brucei* indicating that G4 structures could be their actual targets. Finally, glucose and mannose conjugation to toxic and potent G4-ligands could be an effective strategy in tuning down unspecific drug toxicity.

EXPERIMENTAL SECTION

Compound Synthesis and Purity. Compound synthesis was carried out as previously reported.³¹ The purity of all compounds tested was $\geq 95\%$ and was confirmed by reverse phase HPLC by applying different elution systems and detecting the UV absorption.

Oligonucleotides. All oligonucleotides (Table S1) were purchased from Eurogentec (Belgium) and used without further purification for FRET and CD experiments. NMR samples were purified by centrifugation on 5 kDa filters. Oligonucleotide stock solutions (around 500 μM) were prepared in MilliQ water and stored at $-20\text{ }^\circ\text{C}$. The exact stock concentrations were determined from the absorbance at 260 nm. For FRET melting and CD experiments, the compounds were solubilised in MilliQ water at concentrations of either 5 or 10 mM, depending on the solubility of the compound.

FRET-melting assays. The ligand-induced thermal stabilisations ($\Delta T_{1/2}$) were determined from the difference between the temperature of mid-transition measured without and with the appropriate concentration of ligand, with a final oligonucleotide strand concentration of 0.2 μM . Three independent experiments were conducted on a Stratagene Mx3005P real-time PCR equipment using duplicate conditions in 96 well-plates. The excitation wavelength was set to 492 nm and the emission recorded at 516 nm. The temperature profile consisted in an initial stabilisation at 25 °C for 5 min followed by a 1°C by minute increase till 95 °C. The induced stabilisation was measured in 10 mM lithium cacodylate (pH 7.2) supplemented with 10 mM KCl and 90 mM LiCl.

Circular dichroism (CD) spectroscopy. CD-spectra were recorded at 25°C on a Jasco J-815 equipped with a Peltier temperature controller. Each spectrum corresponds to the average of three scans measured in 1-cm path-length quartz cells at 100 nm min^{-1} (bandwidth: 2 nm, data integration time: 1s). The oligonucleotides were pre-folded at 4 μM in 10 mM lithium cacodylate (pH 7.2) and with the relevant amount of KCl or NaCl. The ligand concentration was adapted to reach the desired ratio (between 1:0 and 1:10), in 100 mM KCl.

Cell Culture. MRC5 cells were maintained at 37 °C and 5 % CO_2 in 100% of humidity in low glucose (1 g/L) DMEM supplemented with 10% heat-inactivated fetal bovine serum (hiFBS), 100 U/ml penicillin and 100 mg/ml streptomycin.

In vitro antitrypanosomal activity. Bloodstream forms (BSF) of *T. brucei brucei* 'single marker' S427 (S16) were grown at 37 °C, 5% CO_2 in HMI-9 medium supplemented with 10% hiFBS. Drug susceptibility assay was performed as described in Carvalho *et al.*⁴⁸ Briefly, parasites (1×10^4 BSF per mL) were incubated in 96-well plates with increasing concentration of drugs/compounds for 72 h at 37 °C, 5% CO_2 in culture medium. Cell proliferation was determined using the alamarBlue® assay⁴⁹ to determine drug sensitivity of African trypanosomes (*T. brucei brucei*) *in vitro*. Fluorescence was recorded with an Infinite® F200 microplate reader (Tecan Austria GmbH, Austria) equipped with 550 and 590 nm filters for excitation and emission wavelengths, respectively.

In vitro antileishmanial activity. The experiments of drug susceptibility on *L. major* (MHOM/IL/80/Friedlin) were carried out as described previously.⁵⁰ Briefly, 1×10^6 promastigotes per mL

were incubated for 72 h at 28 °C in 96-well plates in modified RPMI-1640 medium (Invitrogen, Carlsbad, CA) plus 10 % hiFBS, containing increasing concentration of drugs. Cell proliferation was determined using a MTT-based assay⁵¹. The absorbance was measured at a wavelength of 540 nm.

In vitro antimalarial activity. Drug effects on *in vitro* *P. falciparum* growth were measured in microtiter plates according to Desjardins *et al.*⁵² The final volume in each well was 200 µl, consisting of 50 µl of complete medium (RPMI 1640 + 10% AB human serum) without (controls) or with drug and 150 µl of *P. falciparum*-infected erythrocyte (3D7 strain) suspension (1.5% final hematocrit and 0.6% parasitemia). The drugs dissolved in DMSO, were diluted in complete medium so that the final DMSO concentration never exceeded 0, 25%. After 48 h incubation at 37°C, 30 µl of complete medium containing 0.6µCi [3H]-hypoxanthine were added to each well. After 18 h at 37°C, cells were lysed using an automatic cell harvester and the parasite macromolecules, including radioactive nucleic acids, were retained onto glass fiber filters. The filters were counted for radioactivity, after adding scintillation cocktail, in a liquid scintillation spectrometer. Radioactivity background was obtained from incubation of non-infected erythrocytes under the same condition, and deduced. Parasitic viability was expressed as IC₅₀ which is the drug concentration leading to 50% parasite growth inhibition.

Cytotoxicity assay. MRC5 cells were harvested by trypsinization (0.25%) and seeded in 96 well plates (5000 cells in 100 µL /well) in the presence of increasing concentrations of NDI-compounds. Cellular toxicity was determined using the colorimetric MTT-based assay after incubation at 37 ° C for or 72 h.⁵¹ The results are expressed as the concentration of compound that reduces cell growth by 50% versus untreated control cells (IC₅₀).

Zebrafish toxicity. Acute toxicity assay were carried out by Zeclinics (Barcelona, Spain). Lyophilized compounds were dissolved in 100% DMSO. DMSO volume was calculated for a 100 mM stock solution. To proceed to zebrafish embryo drug incubation, compounds were diluted in 1mL of 0.1% DMSO/E3 Medium to obtain 5 logarithmic concentrations: 0.01µM, 0.1µM, 1µM, 10µM and 100µM (for drugs 1, 2, 3, 4, 5, 6, 7) and 0.1µM, 1µM, 10µM, 100µM and 1mM (for drugs 8,9,10).

Zebrafish embryos preparation: Fertilized embryos of zebrafish (*Danio rerio*), strain AB, were collected in E3 medium in Petri dishes. At 3 hours post fertilization (hpf), after abnormal or not fertilized embryos were

discarded, 20 healthy embryos per condition were placed in wells of a 24-wells plate. Once embryos were placed in each well, E3 medium was replaced by the different dilutions prepared previously for every compound and concentration.

Acute toxicity assay: Embryos were grown from 3 hpf to 96 hpf at 28.5°C. At 96 hours* after treatment mortality LC₅₀ will be determined: LC₅₀ (median lethal dose), calculated by fitting sigmoidal curve to mortality data ($y = \text{Bot} + (\text{Top} - \text{Bot}) / (1 + 10^{-(k \cdot (x_0 - \text{Log}(C)))})$). Bot, minimum mortality; Top, maximum mortality; k, curve slope; x₀, LC₅₀ estimated.

Negative control**: 0.1% DMSO, in three replicates. Positive controls: 4-Diethylamino-benzaldehyde (DEAB) at 5 different concentrations (0.1µM, 1µM, 10µM, 100µM, 1mM). DEAB is a competitive inhibitor of aldehyde dehydrogenases known to generate toxic and teratogenic effects.

* At 24h coagulated eggs were removed from the well to avoid contamination of E3 medium due to tissue decomposition. ** If negative control cumulative mortality is greater than 20% the experiment was not considered significant and had to be repeated.

Absorption and fluorescence spectra: Absorption and emission spectra were recorded in $1.0\text{-}1.5 \times 10^{-5}$ M aqueous solutions (buffered at pH 7.4, 1×10^{-3} M TRIS-HCl) on a JASCO V-550 UV/VIS spectrophotometer and on a Perkin-Elmer LS-65 fluorometer, respectively. The molar absorptivity has been calculated applying the Beer–Lambert relationship to three independent measurements. Fluorescence spectra were measured using 1 nm steps and 0.5-1 s dwell time. Right angle detection was used. All the measurements were carried out at 22°C in quartz cuvettes with path length of 1 cm. The fluorescence spectra were measured in air-equilibrated solutions absorbing less than 0.1 at all wavelengths to avoid inner filter effects and re-absorption of emission.

Confocal microscopy. *T. brucei* parasites were incubated with 5 µM of NDI compounds in 0.5 mL of each respective medium for 30 and 150 min at 37 °C and 100 % of humidity. Then, the parasites were fixed with paraformaldehyde 4% for 30 min, washed twice in cold phosphate-buffered saline (PBS) and processed by microscope observation. Images were acquired using a Leica SP5 confocal microscope (exciting at 488 nm and detecting the emission between 540 and 650 nm), while the images were deconvoluted using Huygens

Professional image processing software from Scientific Volume Imaging (<http://www.svi.nl>). The merge of the images were made with Fiji software (<https://fiji.sc/>).

ASSOCIATED CONTENT

Supporting Information

The Supporting Information is available free of charge on the ACS Publications website.

DNA sequences used in the present study; PQS density found per chromosome of each parasite examined; CD spectra of EBR1 in the absence and presence of different concentrations of Na⁺; CD experiments with EBR1mut sequence; imino region of NMR spectra for EBR1 at different temperatures; characterization of EBR1-FT sequence: a) CD spectra in the absence and presence of different concentrations of K⁺. b) UV-monitored thermal denaturation experiment; FRET-melting stabilization induced by compounds **6** and **7** on EBR1-FT G-quadruplex; absorption and emission spectra of **6** and **7** in water; zebra fish embryo graphs concentration-mortality response (PDF)

Molecular formula strings and associated biological data (CSV)

AUTHOR INFORMATION

Corresponding Authors

*J.M.P-V.: phone, +34-958181685; e-mail, josepv@ipb.csic.es

*J.C.M.: phone, +34-958181644; e-mail, jcmorales@ipb.csic.es

ACKNOWLEDGEMENTS

This work was supported by the Spanish Ministerio de Economía y Competitividad (CTQ2012-35360, CTQ2015-64275-P, and SAF2016-80228-R), Junta de Andalucía (BIO1786), Worldwide Cancer Research Foundation (16-0290), Italian Association for Cancer Research (AIRC, IG2013-14708), Agence Nationale de la Recherche (ANR Quarpdien, ANR-12-BSV8-0008-01), the SYMBIT project (reg. no. CZ.02.1.01/0.0/0.0/15_003/0000477) financed by the ERDF and FEDER funds from the EU are gratefully

acknowledged. M.A.R. and M.M.G. thanks Ministerio de Educación, Cultura y Deporte for a FPU and a FPI predoctoral fellowship, respectively. EBR is a student of the Pharmacy PhD program of the University of Granada (Spain).

ABBREVIATIONS

PQS, Putative G-quadruplex forming sequence, carb-NDI; carb-NDI, carbohydrate conjugated naphthalene diimide; hTel, human telomerase DNA sequence; VSG, variable surface glycoprotein ; ORF, open reading frames; GLUT, glucose transporter; CD, circular dichroism; TDS, thermal difference spectroscopy; IDS, Isothermal difference spectroscopy; FRET, Förster resonance energy transfer; SI, selectivity index; NDI, naphthalene diimide.

REFERENCES

1. (a) Huppert, J. L.; Bugaut, A.; Kumari, S.; Balasubramanian, S. G-quadruplexes: the beginning and end of UTRs. *Nucleic Acids Res.* **2008**, *36* (19), 6260-6268; (b) Huppert, J. L. Four-stranded nucleic acids: structure, function and targeting of G-quadruplexes. *Chem. Soc. Rev.* **2008**, *37* (7), 1375-1384; (c) Balasubramanian, S.; Neidle, S. G-quadruplex nucleic acids as therapeutic targets. *Curr. Opin. Chem. Biol.* **2009**, *13* (3), 345-353; (d) Neidle, S. The structures of quadruplex nucleic acids and their drug complexes. *Curr. Opin. Struct. Biol.* **2009**, *19* (3), 239-250; (e) Bedrat, A.; Lacroix, L.; Mergny, J. L. Re-evaluation of G-quadruplex propensity with G4Hunter. *Nucleic Acids Res.* **2016**, *44* (4), 1746-1759.
2. (a) Chambers, V. S.; Marsico, G.; Boutell, J. M.; Di Antonio, M.; Smith, G. P.; Balasubramanian, S. High-throughput sequencing of DNA G-quadruplex structures in the human genome. *Nat. Biotech.* **2015**, *33* (8), 877-881; (b) Huppert, J. L.; Balasubramanian, S. Prevalence of quadruplexes in the human genome. *Nucleic Acids Res.* **2005**, *33* (9), 2908-2916; (c) Kwok, C. K.; Merrick, C. J. G-Quadruplexes: prediction, characterization, and biological application. *Trends Biotechnol.* **2017**, *35* (10), 997-1013.
3. Rodriguez, R.; Miller, K. M.; Forment, J. V.; Bradshaw, C. R.; Nikan, M.; Britton, S.; Oelschlaegel, T.; Xhemalce, B.; Balasubramanian, S.; Jackson, S. P. Small-molecule-induced DNA damage identifies alternative DNA structures in human genes. *Nat. Chem. Biol.* **2012**, *8* (3), 301-310.

4. (a) Kruisselbrink, E.; Guryev, V.; Brouwer, K.; Pontier, D. B.; Cuppen, E.; Tijsterman, M. Mutagenic capacity of endogenous G4 DNA underlies genome instability in FANCI-defective *C. elegans*. *Curr. Biol.* **2008**, *18* (12), 900-905; (b) Koole, W.; van Schendel, R.; Karambelas, A. E.; van Heteren, J. T.; Okihara, K. L.; Tijsterman, M. A Polymerase Theta-dependent repair pathway suppresses extensive genomic instability at endogenous G4 DNA sites. *Nat. Commun.* **2014**, *5* (3216), 1-10; (c) Castillo Bosch, P.; Segura-Bayona, S.; Koole, W.; van Heteren, J. T.; Dewar, J. M.; Tijsterman, M.; Knipscheer, P. FANCI promotes DNA synthesis through G-quadruplex structures. *EMBO J.* **2014**, *33* (21), 2521-2533; (d) Ohnmacht, S. A.; Neidle, S. Small-molecule quadruplex-targeted drug discovery. *Bioorg. Med. Chem. Lett.* **2014**, *24* (12), 2602-2612; (e) Mendoza, O.; Bourdoncle, A.; Boule, J. B.; Brosh, R. M., Jr.; Mergny, J. L. G-quadruplexes and helicases. *Nucleic Acids Res.* **2016**, *44* (5), 1989-2006.
5. Sarkies, P.; Reams, C.; Simpson, L. J.; Sale, J. E. Epigenetic instability due to defective replication of structured DNA. *Mol. Cell* **2010**, *40* (5), 703-713.
6. Verma, A.; Halder, K.; Halder, R.; Yadav, V. K.; Rawal, P.; Thakur, R. K.; Mohd, F.; Sharma, A.; Chowdhury, S. Genome-wide computational and expression analyses reveal G-quadruplex DNA motifs as conserved cis-regulatory elements in human and related species. *J. Med. Chem.* **2008**, *51* (18), 5641-5649.
7. (a) Hershman, S. G.; Chen, Q.; Lee, J. Y.; Kozak, M. L.; Yue, P.; Wang, L. S.; Johnson, F. B. Genomic distribution and functional analyses of potential G-quadruplex-forming sequences in *Saccharomyces cerevisiae*. *Nucleic Acids Res.* **2008**, *36* (1), 144-156; (b) Johnson, J. E.; Smith, J. S.; Kozak, M. L.; Johnson, F. B. In vivo veritas: Using yeast to probe the biological functions of G-quadruplexes. *Biochimie* **2008**, *90* (8), 1250-1263.
8. (a) Rawal, P.; Kummarasetti, V. B.; Ravindran, J.; Kumar, N.; Halder, K.; Sharma, R.; Mukerji, M.; Das, S. K.; Chowdhury, S. Genome-wide prediction of G4 DNA as regulatory motifs: role in *Escherichia coli* global regulation. *Genome Res.* **2006**, *16* (5), 644-655; (b) Wieland, M.; Hartig, J. S. Investigation of mRNA quadruplex formation in *Escherichia coli*. *Nat. Protoc.* **2009**, *4* (11), 1632-1640.
9. (a) Perrone, R.; Nadai, M.; Frasson, I.; Poe, J. A.; Butovskaya, E.; Smithgall, T. E.; Palumbo, M.; Palu, G.; Richter, S. N. A dynamic G-quadruplex region regulates the HIV-1 long terminal repeat promoter. *J. Med. Chem.* **2013**, *56* (16), 6521-6530; (b) Rajendran, A.; Endo, M.; Hidaka, K.; Tran, P. L.; Mergny, J.

- L.; Gorelick, R. J.; Sugiyama, H. HIV-1 nucleocapsid proteins as molecular chaperones for tetramolecular antiparallel G-quadruplex formation. *J. Am. Chem. Soc.* **2013**, *135* (49), 18575-18585;
- (c) Amrane, S.; Kerkour, A.; Bedrat, A.; Vialet, B.; Andreola, M. L.; Mergny, J. L. Topology of a DNA G-quadruplex structure formed in the HIV-1 promoter: a potential target for anti-HIV drug development. *J. Am. Chem. Soc.* **2014**, *136* (14), 5249-5252; (d) Artusi, S.; Nadai, M.; Perrone, R.; Biasolo, M. A.; Palu, G.; Flamand, L.; Calistri, A.; Richter, S. N. The Herpes Simplex Virus-1 genome contains multiple clusters of repeated G-quadruplex: implications for the antiviral activity of a G-quadruplex ligand. *Antiviral Res.* **2015**, *118*, 123-131.
10. Harris, L. M.; Merrick, C. J. G-quadruplexes in pathogens: a common route to virulence control? *PLoS Pathog.* **2015**, *11* (2), e1004562.
11. Gardner, M. J.; Hall, N.; Fung, E.; White, O.; Berriman, M.; Hyman, R. W.; Carlton, J. M.; Pain, A.; Nelson, K. E.; Bowman, S.; Paulsen, I. T.; James, K.; Eisen, J. A.; Rutherford, K.; Salzberg, S. L.; Craig, A.; Kyes, S.; Chan, M. S.; Nene, V.; Shallom, S. J.; Suh, B.; Peterson, J.; Angiuoli, S.; Pertea, M.; Allen, J.; Selengut, J.; Haft, D.; Mather, M. W.; Vaidya, A. B.; Martin, D. M.; Fairlamb, A. H.; Fraunholz, M. J.; Roos, D. S.; Ralph, S. A.; McFadden, G. I.; Cummings, L. M.; Subramanian, G. M.; Mungall, C.; Venter, J. C.; Carucci, D. J.; Hoffman, S. L.; Newbold, C.; Davis, R. W.; Fraser, C. M.; Barrell, B. Genome sequence of the human malaria parasite *Plasmodium falciparum*. *Nature* **2002**, *419* (6906), 498-511.
12. (a) Stanton, A.; Harris, L. M.; Graham, G.; Merrick, C. J. Recombination events among virulence genes in malaria parasites are associated with G-quadruplex-forming DNA motifs. *BMC Genomics* **2016**, *17* (1), 859; (b) Smargiasso, N.; Gabelica, V.; Damblon, C.; Rosu, F.; De Pauw, E.; Teulade-Fichou, M. P.; Rowe, J. A.; Claessens, A. Putative DNA G-quadruplex formation within the promoters of *Plasmodium falciparum* var genes. *BMC Genomics* **2009**, *10*, 362.
13. Bottius, E.; Bakhsis, N.; Scherf, A. *Plasmodium falciparum* telomerase: de novo telomere addition to telomeric and nontelomeric sequences and role in chromosome healing. *Mol. Cell Biol.* **1998**, *18* (2), 919-925.
14. Dore, E.; Pace, T.; Ponzi, M.; Scotti, R.; Frontali, C. Homologous telomeric sequences are present in different species of the genus *Plasmodium*. *Mol. Biochem. Parasitol.* **1986**, *21* (2), 121-127.

15. (a) Duraisingh, M. T.; Voss, T. S.; Marty, A. J.; Duffy, M. F.; Good, R. T.; Thompson, J. K.; Freitas-Junior, L. H.; Scherf, A.; Crabb, B. S.; Cowman, A. F. Heterochromatin silencing and locus repositioning linked to regulation of virulence genes in *Plasmodium falciparum*. *Cell* **2005**, *121* (1), 13-24; (b) Freitas-Junior, L. H.; Hernandez-Rivas, R.; Ralph, S. A.; Montiel-Condado, D.; Ruvalcaba-Salazar, O. K.; Rojas-Meza, A. P.; Mancio-Silva, L.; Leal-Silvestre, R. J.; Gontijo, A. M.; Shorte, S.; Scherf, A. Telomeric heterochromatin propagation and histone acetylation control mutually exclusive expression of antigenic variation genes in malaria parasites. *Cell* **2005**, *121* (1), 25-36.
16. Claessens, A.; Hamilton, W. L.; Kekre, M.; Otto, T. D.; Faizullabhoj, A.; Rayner, J. C.; Kwiatkowski, D. Generation of antigenic diversity in *Plasmodium falciparum* by structured rearrangement of Var genes during mitosis. *PLoS Genet.* **2014**, *10* (12), e1004812.
17. Scherf, A.; Hernandez-Rivas, R.; Buffet, P.; Bottius, E.; Benatar, C.; Pouvelle, B.; Gysin, J.; Lanzer, M. Antigenic variation in malaria: in situ switching, relaxed and mutually exclusive transcription of var genes during intra-erythrocytic development in *Plasmodium falciparum*. *EMBO J.* **1998**, *17* (18), 5418-5426.
18. (a) Blackburn, E. H.; Challoner, P. B. Identification of a telomeric DNA sequence in *Trypanosoma brucei*. *Cell* **1984**, *36* (2), 447-457; (b) Van der Ploeg, L. H.; Liu, A. Y.; Borst, P., Structure of the growing telomeres of Trypanosomes. *Cell* **1984**, *36* (2), 459-468.
19. (a) Lanzer, M.; Fischer, K.; Le Blancq, S. M. Parasitism and chromosome dynamics in protozoan parasites: is there a connection? *Mol. Biochem. Parasitol.* **1995**, *70* (1-2), 1-8; (b) Crozatier, M.; Van der Ploeg, L. H.; Johnson, P. J.; Gommers-Ampt, J.; Borst, P. Structure of a telomeric expression site for variant specific surface antigens in *Trypanosoma brucei*. *Mol. Biochem. Parasitol.* **1990**, *42* (1), 1-12.
20. Glover, L.; Alford, S.; Horn, D. DNA break site at fragile subtelomeres determines probability and mechanism of antigenic variation in African trypanosomes. *PLoS Pathog.* **2013**, *9* (3), e1003260.
21. (a) Borst, P.; Greaves, D. R. Programmed gene rearrangements altering gene expression. *Science* **1987**, *235* (4789), 658-67; (b) Devlin, R.; Marques, C. A.; McCulloch, R. Does DNA replication direct locus-specific recombination during host immune evasion by antigenic variation in the African trypanosome? *Curr. Genet.* **2017**, *63* (3), 441-449.

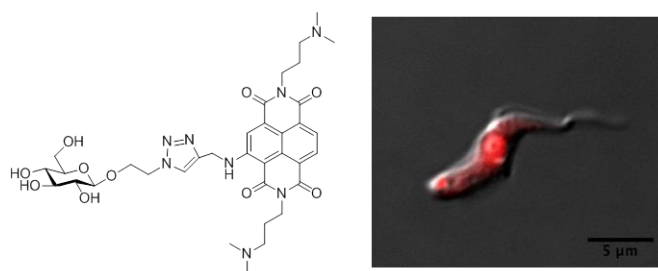
22. Benne, R.; Van den Burg, J.; Brakenhoff, J. P.; Sloof, P.; Van Boom, J. H.; Tromp, M. C. Major transcript of the frameshifted coxII gene from trypanosome mitochondria contains four nucleotides that are not encoded in the DNA. *Cell* **1986**, *46* (6), 819-826.
23. Leeder, W. M.; Hummel, N. F.; Goring, H. U. Multiple G-quartet structures in pre-edited mRNAs suggest evolutionary driving force for RNA editing in trypanosomes. *Sci. Rep.* **2016**, *6*, 29810.
24. Cullen, D. R.; Mocerino, M. A Brief review of drug discovery research for human african Trypanosomiasis. *Curr. Med. Chem.* **2017**, *24* (7), 701-717.
25. Balasubramanian, S.; Hurley, L. H.; Neidle, S. Targeting G-quadruplexes in gene promoters: a novel anticancer strategy? *Nat. Rev. Drug. Discov.* **2011**, *10* (4), 261-275.
26. (a) Davis, J. T. G-quartets 40 years later: from 5'-GMP to molecular biology and supramolecular chemistry. *Angew. Chem. Int. Ed.* **2004**, *43* (6), 668-698; (b) Maji, B.; Bhattacharya, S. Advances in the molecular design of potential anticancer agents via targeting of human telomeric DNA. *Chem. Commun.* **2014**, *50* (49), 6422-6438; (c) Xiong, Y.-X.; Huang, Z.-S.; Tan, J.-H. Targeting G-quadruplex nucleic acids with heterocyclic alkaloids and their derivatives. *Eur. J. Med. Chem.* **2015**, *97*, 538-551.
27. (a) Métifiot, M.; Amrane, S.; Mergny, J.-L.; Andreola, M.-L. Anticancer molecule AS1411 exhibits low nanomolar antiviral activity against HIV-1. *Biochimie* **2015**, *118* (Supplement C), 173-175; (b) Perrone, R.; Doria, F.; Butovskaya, E.; Frasson, I.; Botti, S.; Scalabrin, M.; Lago, S.; Grande, V.; Nadai, M.; Freccero, M.; Richter, S. N. Synthesis, binding and antiviral properties of potent core-extended naphthalene diimides targeting the HIV-1 long terminal repeat promoter G-quadruplexes. *J. Med. Chem.* **2015**, *58* (24), 9639-9652; (c) Biswas, B.; Kandpal, M.; Vivekanandan, P. A G-quadruplex motif in an envelope gene promoter regulates transcription and virion secretion in HBV genotype B. *Nucleic Acids Res.* **2017**, *45* (19), 11268-11280.
28. De Cian, A.; Grellier, P.; Mouray, E.; Depoix, D.; Bertrand, H.; Monchaud, D.; Teulade-Fichou, M. P.; Mergny, J. L.; Alberti, P. Plasmodium telomeric sequences: structure, stability and quadruplex targeting by small compounds. *Chembiochem* **2008**, *9* (16), 2730-2739.
29. Guillon, J.; Cohen, A.; Gueddouda, N. M.; Das, R. N.; Moreau, S.; Ronga, L.; Savrimoutou, S.; Basmaciyan, L.; Monnier, A.; Monget, M.; Rubio, S.; Garnerin, T.; Azas, N.; Mergny, J. L.; Mullie, C.; Sonnet, P. Design, synthesis and antimalarial activity of novel bis{N-[(pyrrolo[1,2-a]quinoxalin-4-yl)benzyl]-3-aminopropyl}amine derivatives. *J. Enzyme Inhib. Med. Chem.* **2017**, *32* (1), 547-563.

30. Calvo, E. P.; Wasserman, M. G-Quadruplex ligands: Potent inhibitors of telomerase activity and cell proliferation in *Plasmodium falciparum*. *Mol. Biochem. Parasitol.* **2016**, *207* (1), 33-38.
31. Arevalo-Ruiz, M.; Doria, F.; Belmonte-Reche, E.; De Rache, A.; Campos-Salinas, J.; Lucas, R.; Falomir, E.; Carda, M.; Perez-Victoria, J. M.; Mergny, J. L.; Freccero, M.; Morales, J. C. Synthesis, binding properties, and differences in cell uptake of G-quadruplex ligands based on carbohydrate naphthalene diimide conjugates. *Chem. Eur. J.* **2017**, *23* (9), 2157-2164.
32. (a) Calvaresi, E. C.; Hergenrother, P. J. Glucose conjugation for the specific targeting and treatment of cancer. *Chem. Sci.* **2013**, *4* (6), 2319-2333; (b) Pohl, J.; Bertram, B.; Hilgard, P.; Nowrousian, M. R.; Stuben, J.; Wiessler, M. D-19575- a sugar-linked isophosphoramidate mustard derivative exploiting transmembrane glucose transport. *Cancer Chemother. Pharmacol.* **1995**, *35* (5), 364-370; (c) Liu, P.; Lu, Y.; Gao, X.; Liu, R.; Zhang-Negrerie, D.; Shi, Y.; Wang, Y.; Wang, S.; Gao, Q. Highly water-soluble platinum(II) complexes as GLUT substrates for targeted therapy: improved anticancer efficacy and transporter-mediated cytotoxic properties. *Chem. Commun.* **2013**, *49* (24), 2421-2423.
33. Burchmore, R. J.; Landfear, S. M. Differential regulation of multiple glucose transporter genes in *Leishmania mexicana*. *J. Biol. Chem.* **1998**, *273* (44), 29118-29126.
34. Rodriguez-Contreras, D.; Feng, X.; Keeney, K. M.; Archie Bouwer, H. G.; Landfear, S. M. Phenotypic characterization of a glucose transporter null mutant in *Leishmania mexicana*. *Mol. Biochem. Parasitol.* **2007**, *153* (1), 9-18.
35. (a) Feng, X.; Rodriguez-Contreras, D.; Buffalo, C.; Bouwer, H. G. A.; Kruvand, E.; Beverley, S. M.; Landfear, S. M. Amplification of an alternate transporter gene suppresses the avirulent phenotype of glucose transporter null mutants in *Leishmania mexicana*. *Mol. Microbiol.* **2009**, *71* (2), 369-381; (b) Rodríguez-Contreras, D.; Landfear, S. M. Metabolic Changes in Glucose Transporter-deficient *Leishmania mexicana* and Parasite Virulence. *J. Biol. Chem.* **2006**, *281*, 20068-20076.
36. Woodrow, C. J.; Penny, J. I.; Krishna, S. Intraerythrocytic *Plasmodium falciparum* expresses a high affinity facilitative hexose transporter. *J. Biol. Chem.* **1999**, *274* (11), 7272-7277.
37. Barrett, M. P.; Tetaud, E.; Seyfang, A.; Bringaud, F.; Baltz, T. Trypanosome glucose transporters. *Mol. Biochem. Parasitol.* **1998**, *91* (1), 195-205.
38. Kikin, O.; D'Antonio, L.; Bagga, P. S. QGRS Mapper: a web-based server for predicting G-quadruplexes in nucleotide sequences. *Nucleic Acids Res.* **2006**, *34* (Web Server issue), W676-682.

39. Karsisiotis, A. I.; Hessari, N. M.; Novellino, E.; Spada, G. P.; Randazzo, A.; Webba da Silva, M. Topological characterization of nucleic acid G-quadruplexes by UV absorption and circular dichroism. *Angew. Chem. Int. Ed.* **2011**, *50* (45), 10645-8.
40. (a) Diveshkumar, K. V.; Sakrikar, S.; Harikrishna, S.; Dhamodharan, V.; Pradeepkumar, P. I. Targeting promoter G-quadruplex DNAs by indenopyrimidine-based ligands. *ChemMedChem* **2014**, *9* (12), 2754-2765; (b) Perrone, R.; Nadai, M.; Poe, J. A.; Frasson, I.; Palumbo, M.; Palu, G.; Smithgall, T. E.; Richter, S. N. Formation of a unique cluster of G-quadruplex structures in the HIV-1 Nef coding region: implications for antiviral activity. *PLoS One* **2013**, *8* (8), e73121.
41. Mergny, J. L.; Li, J.; Lacroix, L.; Amrane, S.; Chaires, J. B. Thermal difference spectra: a specific signature for nucleic acid structures. *Nucleic Acids Res.* **2005**, *33* (16), e138.
42. Mergny, J. L.; Phan, A. T.; Lacroix, L. Following G-quartet formation by UV-spectroscopy. *FEBS Lett.* **1998**, *435* (1), 74-78.
43. Feigon, J.; Koshlap, K. M.; Smith, F. W. ¹H NMR spectroscopy of DNA triplexes and quadruplexes. *Methods Enzymol.* **1995**, *261*, 225-255.
44. Sipes, N. S.; Padilla, S.; Knudsen, T. B. Zebrafish: as an integrative model for twenty-first century toxicity testing. *Birth Defects Res. C Embryo Today* **2011**, *93* (3), 256-267.
45. Busquet, F.; Strecker, R.; Rawlings, J. M.; Belanger, S. E.; Braunbeck, T.; Carr, G. J.; Cenijn, P.; Fochtman, P.; Gourmelon, A.; Hubler, N.; Kleensang, A.; Knobel, M.; Kussatz, C.; Legler, J.; Lillicrap, A.; Martinez-Jeronimo, F.; Polleichtner, C.; Rzodeczko, H.; Salinas, E.; Schneider, K. E.; Scholz, S.; van den Brandhof, E. J.; van der Ven, L. T.; Walter-Rohde, S.; Weigt, S.; Witters, H.; Halder, M. OECD validation study to assess intra- and inter-laboratory reproducibility of the zebrafish embryo toxicity test for acute aquatic toxicity testing. *Regul. Toxicol. Pharmacol.* **2014**, *69* (3), 496-511.
46. (a) Ledoux, A.; St-Gelais, A.; Cieciewicz, E.; Jansen, O.; Bordignon, A.; Illien, B.; Di Giovanni, N.; Marvilliers, A.; Hoareau, F.; Pendeville, H.; Quetin-Leclercq, J.; Frederich, M. Antimalarial activities of alkyl cyclohexenone derivatives isolated from the leaves of *Poupartia borbonica*. *J. Nat. Prod.* **2017**, *80* (6), 1750-1757; (b) Teijeiro-Valino, C.; Yebra-Pimentel, E.; Guerra-Varela, J.; Csaba, N.; Alonso, M. J.; Sanchez, L. Assessment of the permeability and toxicity of polymeric nanocapsules using the zebrafish model. *Nanomedicine* **2017**, *12* (17), 2069-2082.

47. Ali, S.; van Mil, H. G.; Richardson, M. K. Large-scale assessment of the zebrafish embryo as a possible predictive model in toxicity testing. *PLoS One* **2011**, *6* (6), e21076.
48. Carvalho, L.; Martinez-Garcia, M.; Perez-Victoria, I.; Manzano, J. I.; Yardley, V.; Gamarro, F.; Perez-Victoria, J. M. The oral antimalarial drug tafenoquine shows activity against *Trypanosoma brucei*. *Antimicrob. Agents Chemother.* **2015**, *59* (10), 6151-6160.
49. Raz, B.; Iten, M.; Grether-Buhler, Y.; Kaminsky, R.; Brun, R. The Alamar Blue assay to determine drug sensitivity of African trypanosomes (*T.b. rhodesiense* and *T.b. gambiense*) in vitro. *Acta Trop* **1997**, *68* (2), 139-147.
50. Perez-Victoria, J. M.; Bavchvarov, B. I.; Torrecillas, I. R.; Martinez-Garcia, M.; Lopez-Martin, C.; Campillo, M.; Castanys, S.; Gamarro, F. Sitamaquine overcomes ABC-mediated resistance to miltefosine and antimony in *Leishmania*. *Antimicrob. Agents Chemother.* **2011**, *55* (8), 3838-3844.
51. Mosmann, T. Rapid colorimetric assay for cellular growth and survival: application to proliferation and cytotoxicity assays. *J. Immunol. Methods* **1983**, *65* (1-2), 55-63.
52. Desjardins, R. E.; Canfield, C. J.; Haynes, J. D.; Chulay, J. D. Quantitative assessment of antimalarial activity in vitro by a semiautomated microdilution technique. *Antimicrob. Agents Chemother.* **1979**, *16* (6), 710-718.

TABLE OF CONTENTS GRAPHIC



IC_{50} *T.brucei* = 0.017 ± 0.009 μM, SI = 41.8